sustainability

MDPI

Article

Development and Characterization of KOH-Activated Carbons Derived from Zeolite-Catalyzed Pyrolysis of Waste Tires

Camila Aguilar-Ccuno [1], Rossibel Churata [2], Kattia Martínez [3] and Jonathan Almirón [1,*]

[1] Professional School of Environmental Engineering, Faculty of Process Engineering, National University of San Agustín of Arequipa, Santa Catalina Street No. 117, Arequipa 04001, Peru; caguilarcc@unsa.edu.pe
[2] Professional School of Materials Engineering, Faculty of Process Engineering, National University of San Agustín of Arequipa, Santa Catalina Street No. 117, Arequipa 04001, Peru; rchurataa@unsa.edu.pe
[3] Professional School of Chemistry, Faculty of Natural and Formal Sciences, National University of San Agustín of Arequipa, Santa Catalina Street No. 117, Arequipa 04001, Peru; kmartinezr@unsa.edu.pe
* Correspondence: jalmiron@unsa.edu.pe

Abstract: This study focuses on the production and characterization of activated carbons derived from the carbonaceous residue obtained through the catalytic pyrolysis of waste tires. A catalytic pyrolysis process was conducted at 450 °C and 575 °C, employing two zeolitic catalysts, the commercial ZSM-5 and a synthesized zeolite (PZ2), developed from natural pozzolan, which played a key role in the pyrolysis performance and the quality of the resulting carbons. After pyrolysis, the solid residues were chemically activated using KOH to improve their porous structure and surface characteristics. Comprehensive characterization was carried out, including textural properties (BET surface area and porosity) and morphological (SEM) analysis of the activated carbons, as well as crystallinity evaluation (XRD) of the zeolitic catalysts. The BET surface areas of activated carbons PZ2-T1-AK and PZ2-T2-AK reached 608.65 m^2/g and 624.37 m^2/g, respectively, values that surpass those reported for similar materials under comparable activation conditions. The developed porous structure suggests strong potential for applications in adsorption processes, including pollutant removal. These findings demonstrate the effectiveness of zeolite-catalyzed pyrolysis, particularly using PZ2, as a sustainable strategy for transforming tire waste into high-performance adsorbent materials. This approach supports circular economy principles through innovative waste valorization and offers a promising solution to an environmental challenge.

Keywords: waste tires; pyrolysis; zeolite catalyst; activated carbon; chemical activation; waste valorization

check for updates

Academic Editor: Maurizio Volpe

Received: 3 April 2025
Revised: 19 May 2025
Accepted: 20 May 2025
Published: 23 May 2025

Citation: Aguilar-Ccuno, C.; Churata, R.; Martínez, K.; Almirón, J. Development and Characterization of KOH-Activated Carbons Derived from Zeolite-Catalyzed Pyrolysis of Waste Tires. *Sustainability* **2025**, *17*, 4822. https://doi.org/10.3390/su17114822

Copyright: © 2025 by the authors. Licensee MDPI, Basel, Switzerland. This article is an open access article distributed under the terms and conditions of the Creative Commons Attribution (CC BY) license (https://creativecommons.org/licenses/by/4.0/).

1. Introduction

Approximately 2.4 billion tires are produced and sold worldwide each year [1], ranging from public transport vehicles to industrial machinery. It has been identified that one of the main problems related to the mass production of tires is the large amount of waste produced; a significant proportion (around 50%) of the total tires produced ends their useful life as unrecoverable waste [2]. This issue is exacerbated by the non-biodegradable nature of tires, which take between 800 and 1000 years to decompose [3]. The improper disposal of waste tires (WTs) poses a significant risk to public health and the environment. Accumulated WTs can become breeding grounds for disease vectors [4], as stagnant water promotes mosquito proliferation, facilitating the spread of diseases like dengue, Zika, and chikungunya. They also attract rodents and insects, increasing the risk of infections such as

leptospirosis, hantavirus, and salmonellosis [5]. Additionally, WTs are highly flammable and pose a serious fire hazard to surrounding populations [6]. This situation highlights a significant environmental challenge, as the massive disposal of tires has direct negative consequences for natural ecosystems and environmental quality. The improper disposal of non-recyclable waste can lead to soil and water contamination, as well as the release of toxic compounds and pollutants into the atmosphere, thereby contributing to climate change and other environmental problems [4].

To face these problems, innovative and sustainable approaches are needed to man-age this waste and mitigate its adverse effects. Various technologies and methods exist to harvest and reuse WTs, including mechanical recycling, reuse in infrastructure, gasification, and incineration [7]. Mechanical recycling involves shredding tires into crumb rubber for secondary products; however, it does not recover energy or valuable chemicals, limiting resource efficiency. Additionally, reusing tires in infrastructure such as roadbeds or retaining walls offers a practical solution but is limited by its inability to extract energy or high-value materials, often being considered a low-value application. Gasification and incineration are thermal processes that can convert WTs into energy, but both are often criticized for their high operating temperatures, lower selectivity, and potential emission of harmful pollutants [7]. In contrast, emerging thermochemical processes such as pyrolysis offer more sustainable alternatives by maximizing resource recovery, reducing dependence on fossil fuels, and lowering the overall environmental impact. These processes can extract both energy and valuable materials, aligning with circular economy principles [8]. Compared to incineration, WT pyrolysis is considered a more environmentally friendly and economically competitive method, generating three valuable products: fuel gas, oil, and carbon [9–11]. Additionally, pyrolysis meets three essential principles of solid waste management: volume reduction, resource recovery, and pollutant emission mitigation. The high energy intensity of WTs has also encouraged their reuse through thermochemical processes, especially pyrolysis, which enables the generation of alternative fuels and materials, contributing to energy independence and environmental sustainability [8].

Despite being a relatively good method for recycling used tires, the conventional pyrolysis of used tires is subject to certain limitations due to its dependence on impurities such as sulfur in the obtained pyrolytic oil [12]. This issue can limit the direct use of pyrolytic oil in engines or refineries without further treatment [8]. To overcome these challenges, catalytic pyrolysis has gained attention as an approach to enhance the efficiency and selectivity of the process. Various types of catalysts, including natural zeolite, have been used to improve the quantity and quality of oils from tires in catalytic pyrolysis [12,13]. Strong solid acid catalysts like zeolites facilitate thermal decomposition at relatively lower temperatures, shifting product distribution toward lighter, more valuable hydrocarbons in the boiling range of fuel oil. This makes catalytic pyrolysis more economically viable and environmentally sound by improving product quality and reducing energy consumption [14]. The distribution of pyrolytic products typically consists of gas (20%), liquid (35%), carbon black (33%), and metallic residue (12%) by mass [15]. However, such proportions vary depending on factors such as the type of pyrolysis reactor [16], the operating conditions [17] (temperature, pressure, residence time, carrier gas (N_2 or CO_2), particle size, and catalyst), and other factors such as the original composition of the tire [18]. In this sense, a key factor in the present research is the use of zeolites as catalysts, whether commercial or synthesized. This is because some researchers have stated that the addition of zeolite catalysts in the WT pyrolysis process promotes a change in the yield of pyrolytic products [14,19], so the appropriate catalyst can be chosen according to the purpose of the research. For instance, Razzaq and Majeed [20] found that the effects of ZSM-5 and HY zeolite catalyst were a decreased oil yield and an improved gas yield. Olazar et al. [21]

concluded that the catalyst has a significant effect on product fraction distribution and composition, which are very sensitive to the shape selectivity of the zeolite catalyst in the range of 425–500 °C. Suhartono et al. [19] obtained oil and char weight ratios of 36.63% and 47.91%, respectively, at 450 °C in a tubular reactor. The use of zeolites has proven effective in reducing the formation of undesirable compounds, such as sulfur-containing species, in the liquid fraction. This improvement may enhance the commercial value of the pyrolytic oil and decrease the need for extensive post-treatment.

Among the three main byproducts obtained from waste tire pyrolysis, carbon black stands out for its wide industrial applicability and superior quality compared to commercial variants such as semi-reinforced carbon, thanks to the characteristics conferred by the pyrolytic process [22,23]. The quality of this solid residue depends on operational variables such as temperature, residence time, and pressure. In research on WT pyrolysis, the influence of parameters such as temperature, tire type, and the presence of a catalyst and residence time, which determine the quality of the solid product obtained, has been studied [16,24]. In addition to carbon black, the other pyrolysis products also have valuable uses: the pyrolytic oil can be upgraded into diesel-like fuels or used directly in industrial burners, while the syngas, composed mainly of CO, H_2, CH_4, and other light hydrocarbons, can be recovered for energy generation or to fuel the pyrolysis process itself, enhancing energy efficiency. Likewise, the steel residues can be recovered and recycled in the metallurgical industry, contributing to the circular economy [14]. Moreover, pyrolytic carbon black can be further treated to produce activated carbon, a porous material with high surface area and broad applicability, including water and air purification, energy storage, pollutant removal, gas treatment, and even medical uses [25]. However, the presence of inorganic compounds, particularly ZnO and other metals like Fe, Al, Ca, and Mg, along with high sulfur content, can limit its direct application [26–28]. The presence of these substances together with the high sulfur content limits the solid byproduct, so its use is often restricted [28]. The carbon content of the pyrolytic sediments was the highest, up to 86% by weight, followed by its sulfur and nitrogen contents [28]. Pyrolysis carbons obtained at higher temperatures (700–800 °C) had a lower sulfur content. A lower temperature seemed to cause a high sulfur retention due to the relatively high volatility of sulfur at higher temperatures [29]. From what was reviewed, demineralization is highly recommended, since the removal of minerals promotes the creation of new mesopores and micropores, where these pores act as active sites in a subsequent activation [30]. Likewise, as part of the proposed methodology, a chemical activation of the carbon residue will be carried out. In the chemical activation process, various chemical reagents are used to minimize the activation time and temperature, making chemical activation more effective than physical activation. However, corrosiveness and the generation of high pH values are the most considerable drawbacks of this process. Although $ZnCl_2$, NaOH, HNO_3, H_2SO_4, and H_3PO_4 are applied for the activation of carbon residue from tire pyrolysis, K_2CO_3 and KOH are commonly used due to their effective technical performance in increasing the surface area and microvolume [31]. KOH was chosen due to its high efficiency in improving porosity and developing a highly microporous structure. KOH promotes the removal of impurities and the expansion of the pore network, which significantly increases the surface area and microvolume of the activated carbon. Furthermore, its use minimizes the generation of hazardous waste compared to other activators such as $ZnCl_2$, which can generate toxic waste, or H_3PO_4, which requires extensive washing to remove phosphorus residues. Compared to NaOH, KOH shows greater efficiency in creating well-developed pores and better thermal stability during activation, thus optimizing the final quality of the activated carbon [31].

This study addresses a current research gap in the field of waste tire valorization by exploring the catalytic pyrolysis pathway not only as a means for energy recovery but also for the generation of value-added materials. The novelty of this work lies in the strategic

use of zeolite-based catalysts, particularly the use of a synthesized zeolite derived from natural pozzolan, as a means to enhance the quality of the carbonaceous residue obtained during WT catalytic pyrolysis. This residue, typically considered a low-value byproduct, is here revalorized into high-quality activated carbon through chemical activation. The specific aim of this study is to evaluate the potential of producing activated carbons with enhanced surface and chemical properties from the solid fraction resulting from the catalytic pyrolysis of WTs. For this purpose, two zeolitic catalysts (a commercial one and a synthesized one) were thoroughly characterized in terms of textural, morphological, and crystalline properties to assess their influence during the pyrolysis process. Subsequently, the carbonaceous residues or waste tire carbon (WTC) obtained from the catalytic pyrolysis were characterized to understand how catalyst type and pyrolysis temperature affect their potential as precursors for activation. Finally, the WTC and the activated carbons were evaluated with respect to their surface area, porosity, burn-off, cation exchange capacity, and morphology, to determine their suitability for environmental or industrial applications in terms of their adsorption capacity. This integrated approach allows a direct link between catalyst design and the development of high-performance activated carbon materials, contributing to the circular economy and the sustainable management of tire waste. It also addresses a key limitation of conventional pyrolysis by proposing a route that maximizes the utility of solid byproducts through the catalyst-driven enhancement of their properties.

2. Materials and Methods

2.1. Materials

The catalysts used were a commercial zeolite and a synthesized one. Both materials were sieved to maintain a particle size of 106 μm using a No. 140 mesh sieve [32], and dried in a Venticell 222 oven (MMM Group, Berlin, Germany) at 100 °C for 24 h prior to use. The commercial zeolite was a ZSM-5 CBV 524G from the Zeolyst International brand (Kansas City, MO, USA). The synthesized zeolite, referred to in this investigation as PZ2, was made from pozzolan, a natural precursor extracted in the city of Arequipa. This region is characterized by a high availability of pozzolanic material due to the surrounding volcanoes, making it an abundant and cost-effective raw material for zeolite synthesis. The pozzolan used was characterized by X-ray fluorescence (XRF) using a Rigaku dispersive fluorescence equipment, model NEX QC + QuantEZ (Austin, TX, USA), identifying high contents of silicon and aluminum oxides in the material (SiO_2—77.90%; Al_2O_3—15.10%; K_2O—3.65%; Fe_2O_3—1.33%; CaO—1.30%; TiO_2—0.265%; Si/Al—9.10%; Others—0.46%), which indicates that this precursor is suitable for zeolite synthesis [33].

The waste tires (WTs) were obtained from a retreading plant in Arequipa. The company provided pre-shredded tires of approximately 5 cm, which were further processed using a Poling plastic shredder to achieve a particle size that passed through a No. 10 mesh sieve (2 mm), in accordance with ASTM E11 [32]. Subsequently, the obtained tire particles were dried in a Venticell 222 oven at 120 °C for 24 h.

For the carbon activation process, KOH from the HiMedia brand was used as the activating agent, and HCl from the J.T. Baker brand was used for washing the activated carbon.

2.2. Preparation of the Synthesized Catalyst PZ2

One of the catalysts used in this study for WT pyrolysis was synthesized via the alkaline fusion/hydrothermal method with concentrated NaOH, based on the procedure described by Mamani et al. [34], using pozzolan as the precursor.

An acid pre-treatment was performed to remove impurities. After crushing and sieving, 50 g of the pozzolan was mixed with 250 mL of 1 M HCl and stirred magnetically at 90 °C for 2 h. The solid was then filtered, rinsed three times with deionized water, and

dried at 110 °C for 24 h. The acid-treated material was mechanically mixed with powdered sodium hydroxide in a 1.2:1 weight ratio (NaOH/material). This mixture was fused in a muffle furnace at 550 °C for 1 h, then cooled to room temperature, and ground to a fine powder. The fused powder was mixed with water at a 1:5 weight ratio and stirred at room temperature for 3 h. The resulting mixture was transferred to a Teflon-lined stainless-steel autoclave and subjected to hydrothermal treatment under static conditions at 90 °C for 12 h. Finally, the solid was cooled, filtered, and washed with 0.5 M HCl until the pH was below 9. The filtered solid was dried at 105 °C for 12 h to remove residual moisture [34].

2.3. Characterization of the Commercial Catalyst and the Synthesized Catalyst

The textural characterization of the samples was conducted using the Brunauer–Emmett–Teller (BET) method with nitrogen gas as the adsorbate, employing a Gemini VII 2390 surface area analyzer (Norcross, GA, USA), under an evacuation rate of 1000 mmHg·min^{-1} and an equilibration time of 5 s [34]. Morphological analysis was carried out via scanning electron microscopy (SEM) using a Hitachi SU8230 scanning electron microscope (Hitachi High-Tech, Tokyo, Japan) with backscattered electrons, acquiring high-resolution images at a scale of 1 µm to evaluate the surface structure of the zeolites [34]. The crystalline structure of the samples was characterized via X-ray diffraction (XRD) using a Rigaku Miniflex 600 diffractometer (Tokyo, Japan), operated at 40 kV and 15 mA. Data were collected over a 2θ range of 3° to 90° [34], and the diffraction patterns were processed using Origin 2025 software.

To estimate the crystallinity, the 'Peak Analyzer' tool within Origin was employed. Specifically, the 'Calculate Peak Area' function was used to determine both the area under the crystalline peaks and the total diffracted area, which corresponds to the sum of the crystalline and amorphous areas. Crystallinity was calculated using the following equation [35]:

$$C(\%) = \frac{A_c}{A_c + A_a} \times 100, \quad (1)$$

where C is the crystallinity, A_c represents the area of the crystalline peaks, and A_a is the area attributed to the amorphous phase in the XRD diffractogram.

2.4. Pyrolysis of Waste Tires (WTs)

The WT pyrolysis process was conducted using a YUDIAN tubular furnace with a double heating zone. The nitrogen (N_2) flow rate was regulated with a Cole-Parmer controller.

According to Lewandowski et al. [16], key factors influencing the quality of the resulting waste tire char (WTC) include the operating temperature and the presence of catalysts. Accordingly, six different carbon samples were obtained using 10 g of WT for each run; only the temperature (in °C) and the presence or absence of zeolite catalyst varied. Table 1 presents these variables along with the respective sample codes.

Table 1. Pyrolysis process parameters according to tire/catalyst ratio and temperature in °C and codification of obtained WTC.

Pyrolysis	Tire/Catalyst (g)	Temperature (°C)	Code
Thermal	---	450 575	TER-T1 TER-T2
Catalytic (commercial zeolite ZSM-5)	10:0.5	450 575	ZM5-T1 ZM5-T2
Catalytic (synthetized zeolite PZ2)	10:0.5	450 575	PZ2-T1 PZ2-T2

To perform the tests, the procedure described below was followed. First, the tube furnace was turned on, and the heating was programmed according to the set temperature,

either 450 °C or 575 °C, maintaining a heating ramp of 10 °C per minute. Subsequently, the previously determined amount of WT and zeolite (used as a catalyst) was weighed using an analytical balance, and the sample was placed in an alumina crucible. Simultaneously, the mass flow controller was set to establish a nitrogen gas flow rate of 250 mL/min, ensuring an oxygen-free and inert atmosphere.

The cooling system was then placed inside an insulating container filled with liquid nitrogen. Once the tube furnace reached the desired temperature, the crucible containing the WT and zeolite was inserted into the quartz tube, maintaining the set temperature for 30 min. A lid and the cooling system were installed at both ends of the quartz tube, ensuring proper nitrogen flow. After the established time, the crucible was removed to allow it to cool to room temperature. It was necessary to wait until the quartz tube and the tubular furnace reached a temperature of 250 °C to properly collect the liquid products from both the cooling system and the quartz tube. The quartz tube was then carefully removed and left to cool for approximately 15 min or until it reached room temperature.

The pyrolysis and subsequent chemical activation processes were performed using the same laboratory installation, which was equipped to operate under controlled thermal conditions and a nitrogen atmosphere. Figure 1 shows the experimental setup used for both pyrolysis and activation stages.



Figure 1. Laboratory setup used for both the pyrolysis and chemical activation processes, including the tubular furnace, nitrogen gas flow controller, and condensation system for the recovery of pyrolytic products.

Finally, the liquid products were collected from the cooling system located in the flask with liquid nitrogen. Additionally, the solid residues from the crucible, the liquids obtained from the quartz tube, and the waxes generated in the cooling system were weighed. Thorough cleaning of both the quartz tube and the cooling system was then conducted to ensure that they were in optimal condition for subsequent experiments.

Once all the byproducts, the solid fraction (WTC), the liquid fraction (pyrolytic oil), and the gases (n-c gas), were collected and weighed, their respective yields were determined based on the initial mass of the waste tire. The calculation method and the statistical treatment of the yield data are detailed below.

The yield of the obtained byproducts, solid char (WTC), pyrolytic oil, and non-condensable gas, was calculated based on the mass ratio between the recovered product and the initial mass of tire waste fed into the reactor, using the following equation:

$$\text{Yield}(\%) = \frac{m_{\text{product}}}{m_{\text{tire}}} \times 100, \quad (2)$$

where m_{product} is the mass (in grams) of the recovered product (WTC, oil, or gas), and m_{tire} is the initial mass (in grams) of tire residue. Each experimental condition was performed in triplicate.

The average yield ($\overline{x}$) was then calculated as follows:

$$\overline{x} = \frac{1}{n}\sum_{i=1}^{n} x_i, \quad (3)$$

where $\overline{x}$ is the mean value, x_i represents the yield value obtained in each repetition, and n = 3 (total number of repetitions).

And the corresponding standard error of the mean was determined using the equation:

$$\text{Standard error} = \frac{\sqrt{\frac{1}{n-1}\sum_{i=1}^{n}(x_i - \overline{x})^2}}{\sqrt{n}} \quad (4)$$

where n = 3 is the number of replicates. The results are presented as mean ± standard error.

2.5. Chemical Activation of WTC with KOH

A portion of the obtained WTC was chemically activated using KOH as a reagent, with the objective of increasing its surface area and adsorption capacity. For this process, the WTC was manually mixed with KOH pellets using a mortar. The WTC: KOH weight ratio was 1:6, based on research by Sirinwaranon et al. [36], who determined that this ratio significantly increased the surface area of the activated carbon. The mixture was then placed in an Alsint alumina crucible.

The WTC: KOH mixture was subsequently subjected to a pyrolysis process in a tubular furnace at a reaction temperature of 700 °C for 2 h, with a heating rate of 10 °C/min. The process was carried out under a N_2 atmosphere with a flow rate of 150 mL/min. Upon completion of activation, the furnace was shut down, and the equipment was allowed to cool to room temperature, maintaining the N_2 flow throughout. Once cooled, the crucible was removed and weighed to determine the degree of activation (burn-off).

The coding for the activated carbons resulting from the precursor WTCs obtained previously is presented in Table 2.

Table 2. Activation process parameters and codification of activated carbons.

WTC Code	Temperature	Precursor Catalyst	Activation Agent	Activated Carbon Code
TER-T1	450	Thermal	KOH	TER-T1-AK
TER-T2	575			TER-T2-AK
ZM5-T1	450	Catalytic (commercial zeolite ZSM-5)		ZM5-T1-AK
ZM5-T2	575			ZM5-T2-AK
PZ2-T1	450	Catalytic (synthetized zeolite PZ2)		PZ2-T1-AK
PZ2-T2	575			PZ2-T2-AK

The burn-off or weight percent of dry ash-free basis (daf) was calculated using the following equation [37]:

$$\text{Burn-off (wt\% daf)} = (w_1 - w_2)/w_1 \times 100 \quad (5)$$

where w_1 and w_2 represent the carbonized mass (daf) before and after the activation process, respectively. *Note:* daf refers to the mass of the sample excluding both moisture and ash content, providing a more accurate measurement of the organic matter involved in the reaction [37].

Subsequently, the activated carbon was washed with 5 M HCl and stirred for 12 h. After stirring, the carbon was filtered and washed with ultrapure water until a neutral pH was achieved. Finally, the resulting sample was dried in an oven at 100 °C for 3 days. The experimental procedure for obtaining KOH-activated carbons is presented in the flowchart shown in Figure 2.

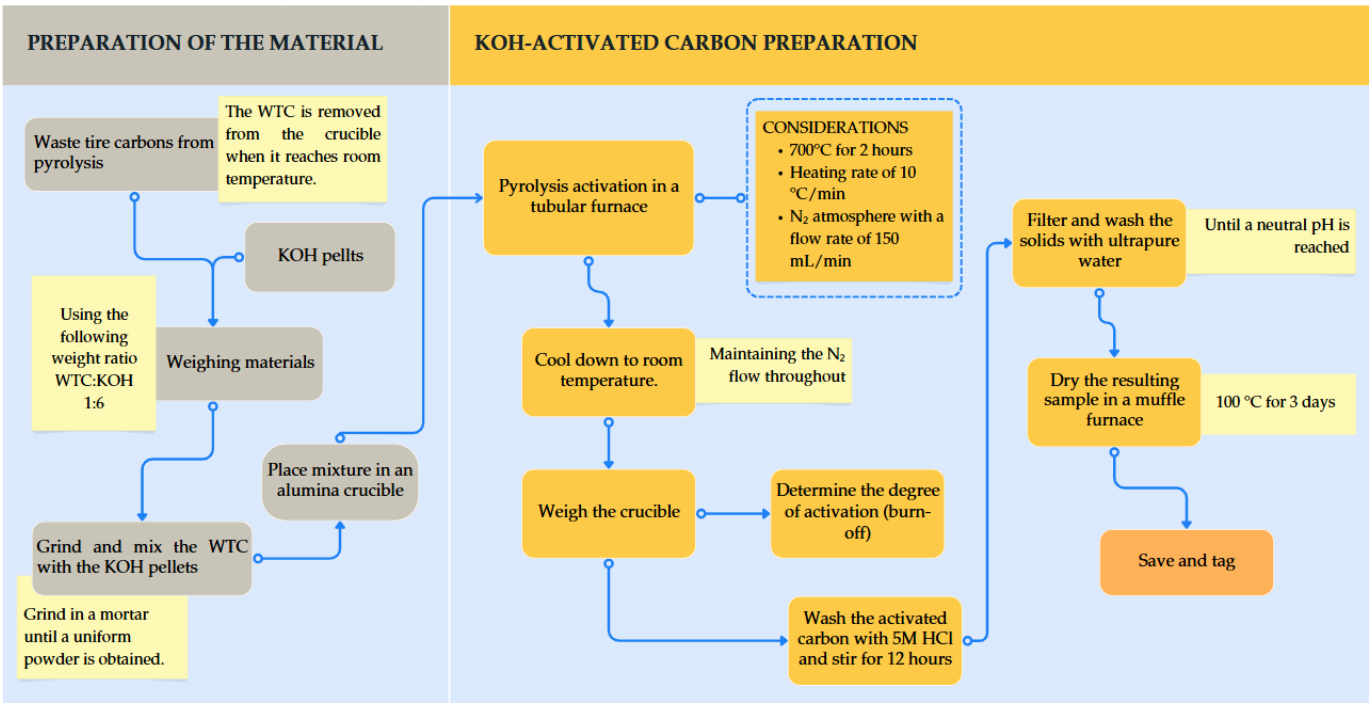


Figure 2. Experimental flowchart illustrating KOH-activated carbon preparation.

2.6. Cation Exchange Capacity Test by the Calcium Chloride Method

A 5 g sample of the activated carbon was weighed and placed in an Erlenmeyer flask, then 20 cc of 1 N $CaCl_2$ was added and stirred for 5 min. The resulting mixture was filtered and the filtrate discarded. The solid residue was washed with 20 cc of distilled water, repeating the process three times and collecting the filtrates, to which 2–3 drops of oxalic acid were added. If a white precipitate formed, the washing process continued until a clear filtrate was obtained, indicating a negative calcium reaction.

The solid was then taken along with the filter paper and placed in a new Erlenmeyer flask, to which 20 cc of 1 N KCl was added and stirred for 5 min. The contents were then filtered, and 5 cc of the filtrate was transferred to another Erlenmeyer flask, along with 1 cc of 4 N NaOH and enough distilled water to fill one-third of the flask. A pinch of murexide indicator was added, and a titration with 0.02 N ethylenediaminetetraacetic acid (EDTA) was performed until the color changed from pinkish-red to violet or lilac, recording the volume used to perform the corresponding calculation.

To calculate the cation exchange capacity (CEC), the following calculations must be considered [38]:

(1) Calcium (Ca) concentration, in milliequivalents per liter (meq/L), is calculated as:

$$1 \text{ meq of Ca} = 20 \text{ mg of Ca} \quad (6)$$

$$1 \text{ meq of EDTA} = 1 \text{ meq of Ca} \quad (7)$$

$$0.02 \text{ N EDTA solution} = 0.02 \text{ Ca solution} \quad (8)$$

$$0.02 \text{ N} = 0.02 \text{ eq/L} = 20 \text{ meq/L} \quad (9)$$

$$X_1 = \frac{20 \times a}{b} \quad (10)$$

where X_1 is the calcium concentration in the extract in units of meq/L, a is the volume of EDTA spent from the filtrate in mL and b is the volume taken from the filtrate in mL.

(2) Calculation of the amount of Ca extracted with 20 mL of KCl solution:

$$X_2 = \frac{X_1 \times 20 \text{ mL}}{1000 \text{ mL}} \quad (11)$$

where X_2 is the amount of Ca extracted in meq, 20 mL is the KCl solution previously added, and 1000 mL is the conversion factor from mL to L.

(3) CEC extrapolated to 100 g of soil:

$$X_3 = \frac{X_2 \times 100 \text{ g}}{5 \text{ g}} \quad (12)$$

where X_3 is CEC in meq/100 g of soil, 100 g is a standard mass reference, and c is the actual mass of soil used in g.

According to the International System of Units (SI), the unit of CEC is cmolc/kg of activated carbon, which is the equivalent of meq/100 g. The CEC classification is presented in Table 3.

Table 3. CEC classification.

CEC Classification ($cmol_c/kg$)	
Very low	<6
Low	6>–<12
Medium	12>–<25
High	35>–<40
Very high	40<

Note: Values extracted from Ćirić et al. [39].

2.7. Characterization of Waste Tire Carbon (WTC) and Activated Carbons

The textural characterization of the samples was conducted using the Brunauer–Emmett–Teller (BET) method with nitrogen gas as the adsorbate, employing a Gemini VII 2390 surface area analyzer, under an evacuation rate of 1000 mmHg·min^{-1} and an equilibration time of 5 s [34]. Morphological analysis was carried out via scanning electron microscopy (SEM) using a Hitachi SU8230 scanning electron microscope (Hitachi High-Tech, Tokyo, Japan), acquiring high-resolution images at a scale of 75,000× to evaluate the surface structure of the zeolites [34].

The whole experimental procedure is summarized in the flowchart presented in Figure 3.

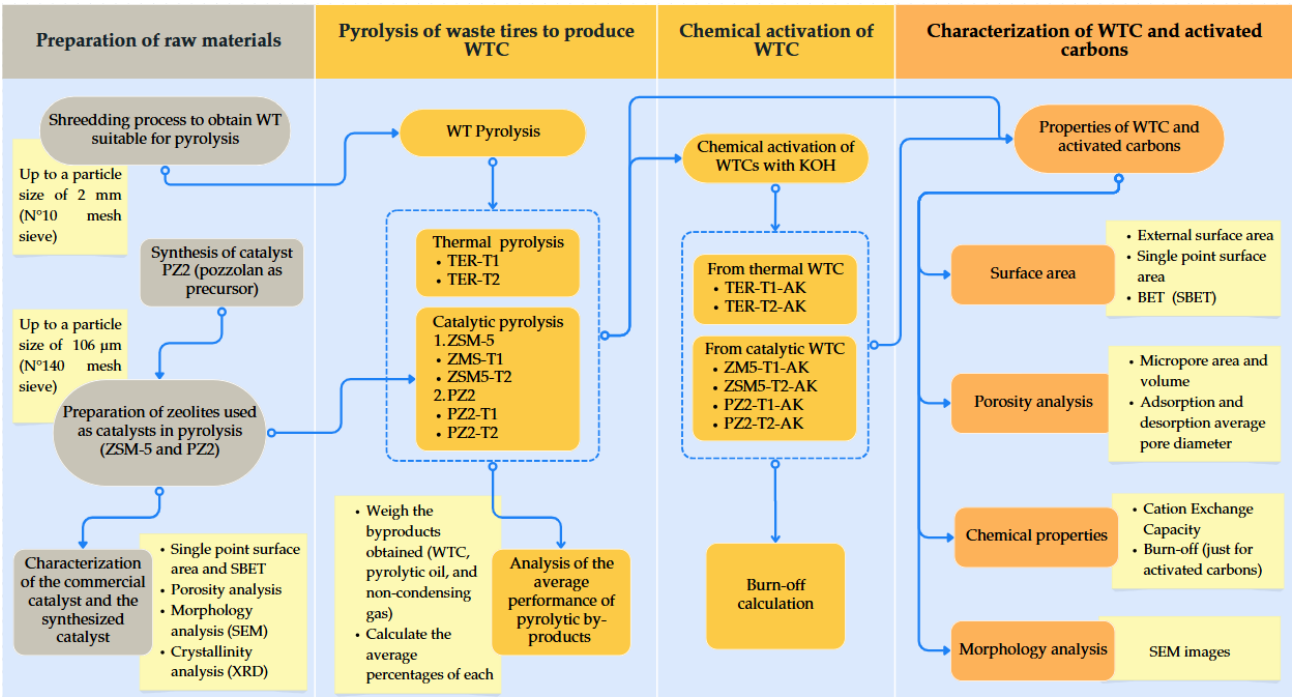


Figure 3. Experimental flowchart illustrating the preparation of raw materials, WT pyrolysis, WTC chemical activation, and the characterization of WTC and the resulting activated carbons.

3. Results

3.1. Characterization of the Catalysts Used in Pyrolysis

3.1.1. Textural Properties of the Catalysts Used in the Production of WTC

One of the influencing factors for the production of WTC, in addition to temperature, was the presence of catalysts during pyrolysis. Therefore, both the textural and chemical properties of the catalysts were evaluated to determine their influence on the properties of the resulting chars and activated carbons. Table 4 summarizes key physical parameters, including single-point surface area, BET surface area, micropore area, micropore volume, and adsorption and average pore diameters (adsorption and desorption). Chemical properties such as CEC and burn-off were also considered.

Table 4. Properties of the catalysts used.

Catalyst	SPSA (m^2/g)	S_{BET} (m^2/g)	M_{area} (m^2/g)	M_{vol} (cm^3/g)	A (nm)	D (nm)	CEC ($cmol_c/kg$)
ZSM-5	205.54	204.55	141.23	0.0735	4.44	6.65	1.1
PZ2	458.50	451.27	408.15	0.2120	6.04	8.63	4.8

Note: Single-point surface area (SPSA), BET surface area (S_{BET}), micropore area (M_{area}), micropore volume (M_{vol}), adsorption average pore diameter (A), desorption average pore diameter (D), and cation exchange capacity (CEC).

The ZSM-5 and PZ2 catalysts exhibit significant differences in their textural and chemical characteristics, which directly affect their performance during pyrolysis and subsequent activation. PZ2 presents higher surface areas (SPSA: 458.50 m^2/g; SBET: 451.27 m^2/g) compared to ZSM-5 (SPSA: 205.54 m^2/g; SBET: 204.55 m^2/g). These values are consistent with the adsorption–desorption isotherms shown in Figure 4. Both isotherms are classified as Type I according to the IUPAC system, indicating a predominantly microporous structure [40]. However, PZ2 exhibits a higher amount of nitrogen adsorbed across all relative pressures (P/P^0), particularly at low $P/P^0 < 0.1$, confirming its greater microporosity and superior adsorption capacity. PZ2 also displays a significantly higher micropore area (408.15 m^2/g vs. 141.23 m^2/g) and micropore volume (0.2120 cm^3/g vs. 0.0735 cm^3/g) than

ZSM-5, indicating its potential to form highly porous carbon structures. Previous studies report a maximum micropore volume of 0.144 cm^3/g for pozzolan-derived zeolites [41], further highlighting the enhanced performance of PZ2 in this study.

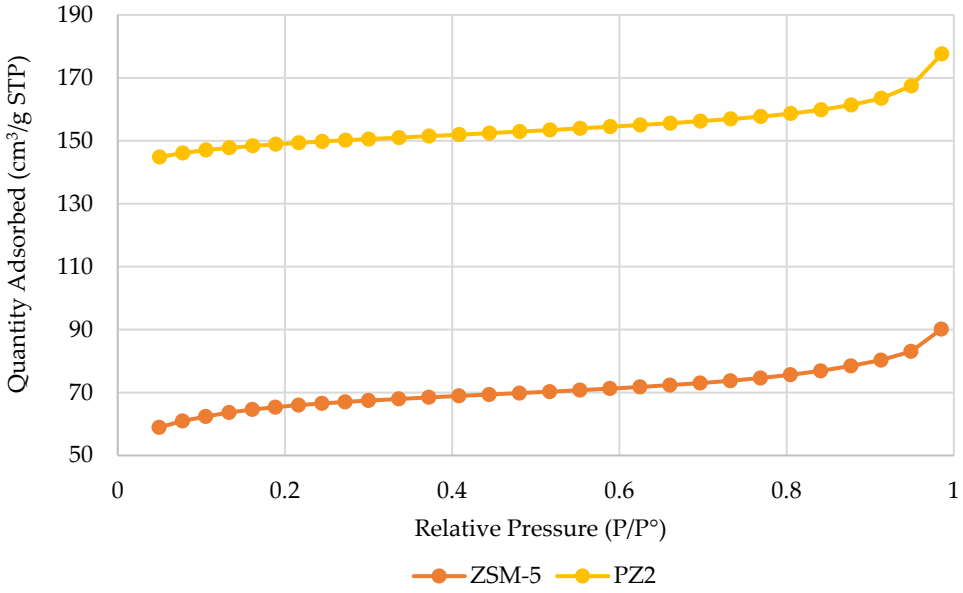


Figure 4. BET/Adsorption–desorption isotherms of N_2 of zeolites ZMS-5 and PZ2.

The difference in micropore area is also notable, with PZ2 showing a value of 408.15 m^2/g, while ZSM-5 reaches only 141.23 m^2/g, indicating that PZ2 has a higher proportion of micropores, a key feature for the formation of highly porous carbons. Likewise, the micropore volume in PZ2 is 0.2120 cm^3/g, which is almost three times greater than that in ZSM-5 (0.0735 cm^3/g), which reinforces PZ2's ability to develop a well-defined porous structure that will favor the adsorption and storage of gases or small molecules in the resulting carbonaceous material [41]. Likewise, it should be emphasized that the PZ2 zeolite, whose precursor is pozzolan, according to previous research, can reach a micropore volume of up to 0.144 cm^3/g [41], which further highlights the capacity of the catalyst to improve the textural properties of the carbons in this study.

Regarding pore size, PZ2 presents average diameters of 6.04 nm in adsorption and 8.63 nm in desorption, compared to 4.44 nm and 6.65 nm for ZSM-5, indicating that PZ2 has a more open and interconnected porosity, favorable for mass transfer during pyrolysis. Although both catalysts show low to very low CEC values according to the classification in the Materials and Methods section [39], PZ2 exhibits a higher CEC than ZSM-5, with more active sites capable of interacting with polar species. This could modify the distribution of chemical species during carbon activation, suggesting that PZ2 can induce greater surface functionalization in the obtained carbons, promoting the presence of oxygenated groups that improve their adsorbent capacity in subsequent applications [39].

3.1.2. Morphological Characterization of Catalysts by Scanning Electron Microscopy (SEM)

Figure 5 presents SEM images of ZSM-5 and PZ2 at 1 µm magnification. ZSM-5 shows a hexagonal morphology with uniform and compact crystalline aggregates and a small particle size, which shows a rough and compact surface [42]. On the other hand, zeolite PZ2 exhibits an octahedral morphology similar to grouped rhombuses, resembling commercial zeolite X [43], with larger and more clustered particles than ZSM-5, which can be clearly seen at a magnification of 1 µm.

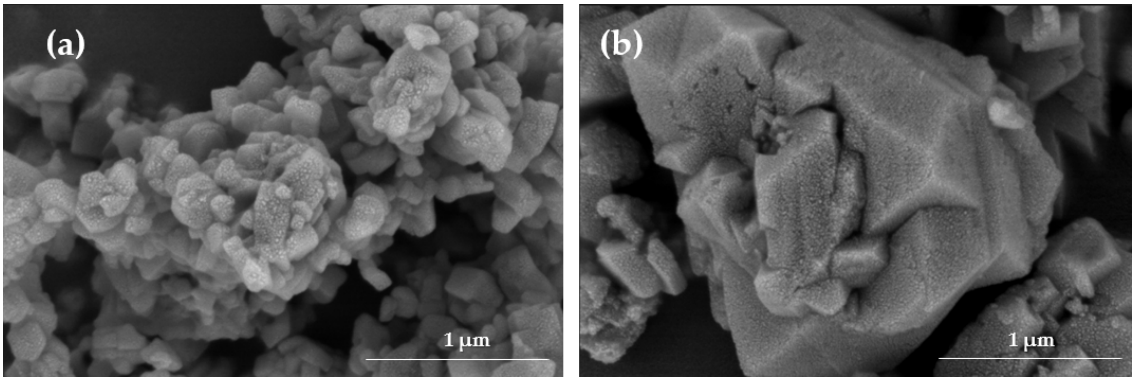


Figure 5. SEM images of the catalysts: (**a**) ZSM-5 at 1 µm and (**b**) PZ2 at 1 µm.

3.1.3. XRD Analysis

The XRD patterns of the ZSM-5 and PZ2 zeolites are shown in Figure 6. According to the graph, some diffraction peaks of PZ2 match those of commercial ZSM-5, specifically those between 7° and 8°, and between 23° and 25° (2-θ), which are peaks associated with said commercial zeolite [44,45].

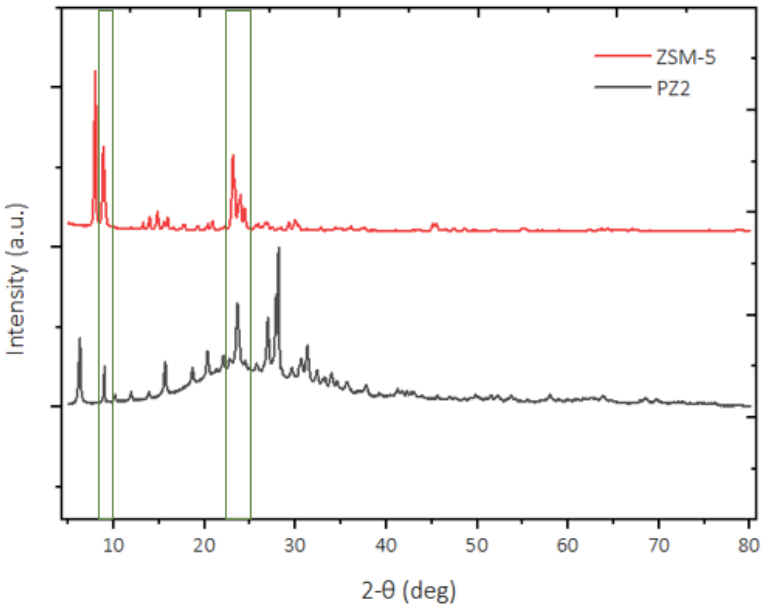


Figure 6. XDR of the catalysts used (top ZSM-5; bottom: PZ2). *Note:* The green lines contain the common peaks between the two zeolites.

Regarding the crystallinity level, ZSM-5 presents higher crystallinity than PZ2, since the latter exhibits a greater proportion of amorphous phases, which are identifiable due to the presence of a characteristic 'hump' in the diffractogram, starting at approximately 15° and ending at 40° in the 2θ range [46]. The calculated crystallinity values corroborate this (according to Equation (1)): 88% for ZSM-5 and 58% for PZ2. These results confirm that PZ2 has a lower degree of crystallinity compared to the commercial zeolite, but despite this, its amorphous aluminosilicate structure makes it thermodynamically metastable and probably exhibits high pozzolanic activity [47].

3.2. Characterization of Byproducts Obtained in Pyrolysis

In order to obtain WTC, the influence of operating conditions on the performance and quality of the resulting material was considered. The first parameter evaluated was temperature, as the yields of the solid, liquid, and gaseous fractions depend on it. There-

fore, average temperatures of 450 °C and 575 °C were used, which are favorable for oil production [40]. These temperatures are also close to 500 °C, the temperature at which the complete conversion of the tire is achieved. Working at lower temperatures, although they may increase the yield of the solid fraction, would result in incomplete tire conversion, negatively affecting the properties of the resulting carbon [48]. The second parameter considered was the presence of catalysts, since these materials enhance and accelerate the pyrolysis process, as well as influencing the quality and applicability of the WTC [49].

Table 5 summarizes the average yield data of the products obtained under different operating conditions. Equations (2) and (3) were applied to determine the average yield of the pyrolytic byproducts, while Equation (4) was used to calculate the standard error associated with the measurements, in accordance with standard statistical procedures. For each WTC sample, three replicates were conducted. The full dataset corresponding to these replicates is presented in the Supplementary Materials (Tables S1 and S2), which provide detailed initial values used for the calculations.

Table 5. Summary of the average yield of waste tire pyrolysis byproducts in the laboratory.

Code	Byproduct Yield (%)		
	WTC	**Pyrolytic Oil**	**n-c Gas**
TER-T1	36.09 ± 0.02	51.95 ± 1.67	11.96 ± 1.59
TER-T2	35.57 ± 0.07	34.20 ± 1.76	30.22 ± 1.69
ZM5-T1	38.32 ± 1.06	49.90 ± 1.34	11.78 ± 1.26
ZM5-T2	35.64 ± 0.10	42.23 ± 2.68	22.13 ± 2.68
PZ2-T1	38.97 ± 0.91	45.65 ± 2.08	15.38 ± 2.97
PZ2-T2	37.61 ± 1.74	41.44 ± 0.63	20.95 ± 2.21

Note: Values show the mean of three replicates ± standard errors. Also, n-c gas refers to non-condensable gas.

WTC yields ranged from 35.57% to 38.97%, with low standard errors (≤1.75%), indicating the stable production of this fraction under the test conditions. Pyrolytic oil yields ranged from 34.20% to 51.95%, showing greater variability in standard errors (0.63–2.68%), suggesting that this byproduct is more sensitive to experimental conditions. In contrast, non-condensable gases exhibited yields between 11.78% and 30.22%, with the highest standard errors (up to 2.97%), reflecting a strong dependence on operating conditions.

Figure 7 below details the effect of temperature and the presence of catalysts on the yield of pyrolytic byproducts.

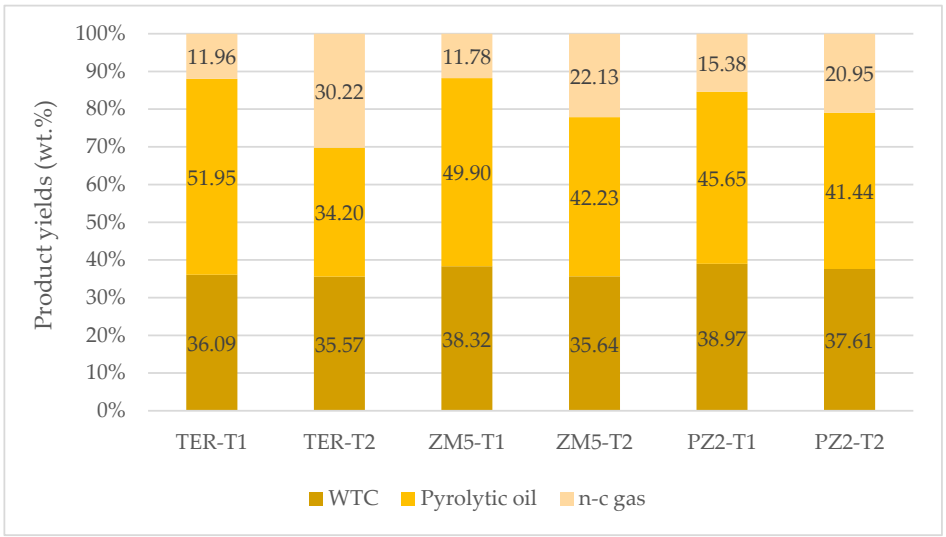


Figure 7. Summary of the average performance of pyrolytic byproducts in the WTC production process.

As shown in Figure 7, WTC yield remained consistent across different pyrolysis conditions. This is because the production of the solid fraction is maximized within the 300–500 °C range; thus, T1 falls within this range, while T2 slightly exceeds it. Although WTC yield does decrease at T2, the reduction is not significant [48].

Furthermore, no variation in solid phase yield was observed due to the presence of catalysts. While catalysts are intended to improve conversion efficiency by enabling lower operating temperatures, they interact more directly with the gaseous and liquid phases [50].

Regarding pyrolytic oil and the gaseous fraction, an inverse relationship was observed between their yields. At moderate temperatures (450–600 °C), a higher yield of the liquid fraction and a lower yield of non-condensable gases were observed [42]. This trend was seen in both the thermal and catalyzed samples, though it was less pronounced in the presence of catalysts. This is because catalysts influence the reaction pathways, controlling secondary reactions such as cracking, which convert liquids into gases [49,50]. The structural stability of the catalysts plays a role in cracking efficiency, as a more stable structure offers well-defined active sites that promote the fragmentation of heavy molecules. In contrast, a less ordered structure may result in a more variable product distribution [50].

3.3. Characterization of Activated Carbons

3.3.1. Properties of WTC and Activated Carbons

The evaluation of the textural and adsorptive properties of activated carbons is essential to determine their material quality. In particular, adsorption capacity is closely related to material performance. Tables 6 and 7 present key physical properties such as external surface area, micropore area, micropore volume, average pore diameter (adsorption and desorption), single-point surface area, and BET surface area. These also include chemical properties such as cation exchange capacity and burn-off. Specifically, Equations (6)–(12) were employed to calculate the CEC values. In the case of burn-off, the corresponding initial values, obtained from three replicate experiments, are presented in Table S3 of the Supplementary Materials.

Table 6. Properties of WTC and activated carbons.

Carbons	ESA (m^2/g)	M_{area} (m^2/g)	M_{vol} (cm^3/g)	A (nm)	D (nm)	CEC ($cmol_c/kg$)
TER-T1	103.32	2.33	0.0004	18.87	19.18	4.4
TER-T2	90.20	9.03	0.0041	13.74	15.22	6.0
ZM5-T1	97.72	16.79	0.0082	18.38	19.40	6.6
ZM5-T2	91.91	17.08	0.0084	19.27	19.26	7.2
PZ2-T1	103.47	1.64	0.0001	16.90	17.89	4.2
PZ2-T2	90.92	7.99	0.4402	17.77	17.93	6.0
TER-T1-AK	321.44	197.96	0.1024	6.97	9.32	12.6
TER-T2-AK	226.90	224.60	0.1166	8.22	10.02	9.0
ZM5-T1-AK	171.68	117.35	0.0608	9.96	12.78	20.4
ZM5-T2-AK	250.32	134.98	0.0697	7.90	10.64	19.2
PZ2-T1-AK	368.07	240.57	0.1248	7.33	11.17	21.0
PZ2-T2-AK	366.84	257.53	0.1337	7.29	11.18	19.2

Note: External surface area (ESA), micropore area (M_{area}), micropore volume (M_{vol}), adsorption average pore diameter (A), desorption average pore diameter (D), and cation exchange capacity (CEC). The codification of the WTCs obtained is given in Table 1 and the codification of activated carbons is provided in Table 2.

According to the values in Table 6, the ESA value of unactivated primary carbons ranged from 90.20 m^2/g (TER-T2) to 103.47 m^2/g (PZ2-T1), indicating a relatively compact initial structure and limited porosity. These traits are typical of carbonized materials prior to activation, and although their adsorption capacity is limited, they provide a suitable

base for developing more functional activated carbons [51]. Activated carbons, on the other hand, showed a substantial increase in ESA, ranging from 171.68 m^2/g (ZM5-T1-AK) to 368.07 m^2/g (PZ2-T1-AK), with PZ2-T1-AK and PZ2-T2-AK presenting the largest areas. This increase reflects the development of a more complex porous structure and larger surface area as a result of the activation process. During activation, non-carbonaceous compounds are removed, and the formation of micro- and mesopores enhances the accessibility of the material's internal surfaces [51]. As noted by Dong et al. [52], activators such as KOH promote reactions in the precursor carbon that facilitate CO release at high pyrolysis temperatures, creating larger pore channels and increasing the external surface area.

Micropore area and volume were also assessed for both unactivated and activated carbons to analyze microporosity development. Unactivated carbons showed relatively low values, with M_{area} ranging from 1.64 m^2/g (PZ2-T1) to 17.08 m^2/g (ZM5-T2), and M_{vol} ranging from 0.000072 cm^3/g (PZ2-T1) to 0.008391 cm^3/g (ZM5-T2). These results indicate minimal microporosity, as expected from carbonized materials prior to activation [51].

After activation, these values increased substantially, with micropore areas reaching up to 240.57 m^2/g (PZ2-T1-AK) and 257.53 m^2/g (PZ2-T2-AK), and micropore volumes reaching 0.1248 cm^3/g (PZ2-T1-AK) and 0.1337 cm^3/g (PZ2-T2-AK). These values were the highest observed, highlighting the effectiveness of KOH activation in enhancing porosity [25]. The PZ2 catalyst also had a notable impact, yielding larger pore areas and volumes than the ZSM-5 catalyst, thus promoting a better porous structure in the respective activated carbons [41].

The average pore diameter values (adsorption and desorption) also showed clear differences between unactivated and activated samples. In unactivated carbons, adsorption pore diameters ranged from 13.74 nm (TER-T2) to 19.27 nm (ZM5-T2), and desorption pore diameters from 15.22 nm (TER-T2) to 19.40 nm (ZM5-T1), corresponding mainly to mesoporous structures typical of carbonaceous materials before activation [53].

Following activation, these values decreased, reflecting a transformation in pore structure where large pores are converted into smaller mesopores. Adsorption pore diameters ranged from 6.97 nm (TER-T1-AK) to 9.96 nm (ZM5-T1-AK), and desorption diameters from 9.32 nm (TER-T1-AK) to 12.78 nm (ZM5-T1-AK). This decrease indicates the success of the treatment in generating a finer and more controlled structure, improving the material's adsorptive properties [48]. The PZ2 catalyst initially displayed more open and interconnected porosity compared to ZSM-5, with larger pore diameters that facilitated reactant diffusion during pyrolysis. After activation, PZ2-derived carbons exhibited a significant reduction in pore size, indicating the structural rearrangement and optimization of their mesoporous network. This transformation enhanced pore accessibility and distribution, increasing adsorptive capacity [53].

Regarding CEC, unactivated carbons showed values between 4.2 $cmol_c/kg$ (PZ2-T1) and 7.2 $cmol_c/kg$ (ZM5-T2), indicating very low to low cation retention capacity, as classified in the Materials and Methods section [39]. These values reflect the limited number of active sites for ion exchange in the initial materials.

After activation, CEC values increased significantly, ranging from 9.0 $cmol_c/kg$ (TER-T2-AK) to 21.0 $cmol_c/kg$ (PZ2-T1-AK). PZ2-derived carbons again stood out, particularly PZ2-T1-AK (21.0 $cmol_c/kg$) and PZ2-T2-AK (19.2 $cmol_c/kg$), which fall into the medium CEC category [43]. This increase is attributed to the formation or exposure of acidic functional groups on the material's surface during activation, enhancing the density of negative charges capable of interacting with cations [39]. The improved CEC suggests higher potential for cation retention, relevant for applications such as the adsorption of heavy metals like Pb^{2+}, Cd^{2+}, and Cu^{2+} [39]. Therefore, the elevated CEC values, especially in samples derived from PZ2, are indicative of their suitability for applications in water treatment and heavy metal remediation.

SPSA and SBET in Table 7 also reflect the significant differences between unactivated and activated carbons, demonstrating the impact of the activation process. In unactivated carbons, SPSA values ranged from 96.70 m^2/g (PZ2-T2) to 112.22 m^2/g (ZM5-T1), and SBET values ranged from 98.91 m^2/g (PZ2-T2) to 114.50 m^2/g (ZM5-T1). These values suggest a moderately developed surface area, though insufficient for highly efficient adsorption [36].

Table 7. Pyrolysis and activation conditions. Properties of WTC and activated carbons obtained, and of different activated carbons produced from tire-derived chars.

Carbons	Reaction Temperature (°C)	Activating Agent	Reaction Time (min)	SPSA (m^2/g)	S_{BET} (m^2/g)	Burn-Off (%)	Ref.
TER-T1	450	-	30	102.40	105.65	-	[This study]
TER-T2	575	-	30	97.16	99.24	-	
ZM5-T1	450	-	30	112.22	114.50	-	
ZM5-T2	575	-	30	107.24	108.99	-	
PZ2-T1	450	-	30	101.84	105.11	-	
PZ2-T2	575	-	30	96.70	98.91	-	
TER-T1-AK	700	KOH	120	516.67	519.40	57.23	
TER-T2-AK	700	KOH	120	451.50	451.51	53.94	
ZM5-T1-AK	700	KOH	120	287.52	289.03	60.06	
ZM5-T2-AK	700	KOH	120	382.55	385.30	64.45	
PZ2-T1-AK	700	KOH	120	604.86	608.65	45.48	
PZ2-T2-AK	700	KOH	120	621.13	624.37	43.68	
WTC 1:6	700	KOH	120	-	114.70	-	[36]
WTC 4M	700	H_3PO_4	120	-	63.07	-	[36]
AC-K	850	KOH	60	184	242	54	[53]
AC-CO_2	800	CO_2	1680	514	720	50	[53]
AC-800	800	KOH	120	-	131	-	[51]
AC-900	900	KOH	120	-	328	-	[51]
C-AC	500	$ZnCl_2$	60	-	86	-	[25]
MC-AC	Microwaved	H_2O_2	15	-	154	-	[25]

Note: Single-point surface area (SPSA); BET surface area (S_{BET}).

Activated carbons, however, exhibited a marked increase, with SPSA values between 287.52 m^2/g (ZM5-T1-AK) and 621.13 m^2/g (PZ2-T2-AK), and S_{BET} values from 289.03 m^2/g (ZM5-T1-AK) to 624.37 m^2/g (PZ2-T2-AK). PZ2-T1-AK and PZ2-T2-AK again exhibited the highest surface areas, confirming their potential for effective adsorption. The development of a greater number of accessible pores significantly improves interaction between the material and target molecules or ions in aqueous media, enhancing the efficiency of adsorption processes [54].

Figure 8 presents the nitrogen adsorption–desorption isotherm analysis (BET), showing that PZ2-T1-AK and PZ2-T2-AK follow a type IV isotherm with a hysteresis loop, combining characteristics of both micropore and mesopore adsorption. The hysteresis indicates mesoporosity, while the initial portion of the isotherm corresponds to micropore adsorption [40].

The development of a porous structure in the activated materials results in increased adsorption capacity, as reflected in their high BET surface area values. For these samples, significant adsorption at low relative pressures indicates dominant microporosity, while the gradual increase at higher pressures corresponds to mesoporosity generated during chemical activation [40].

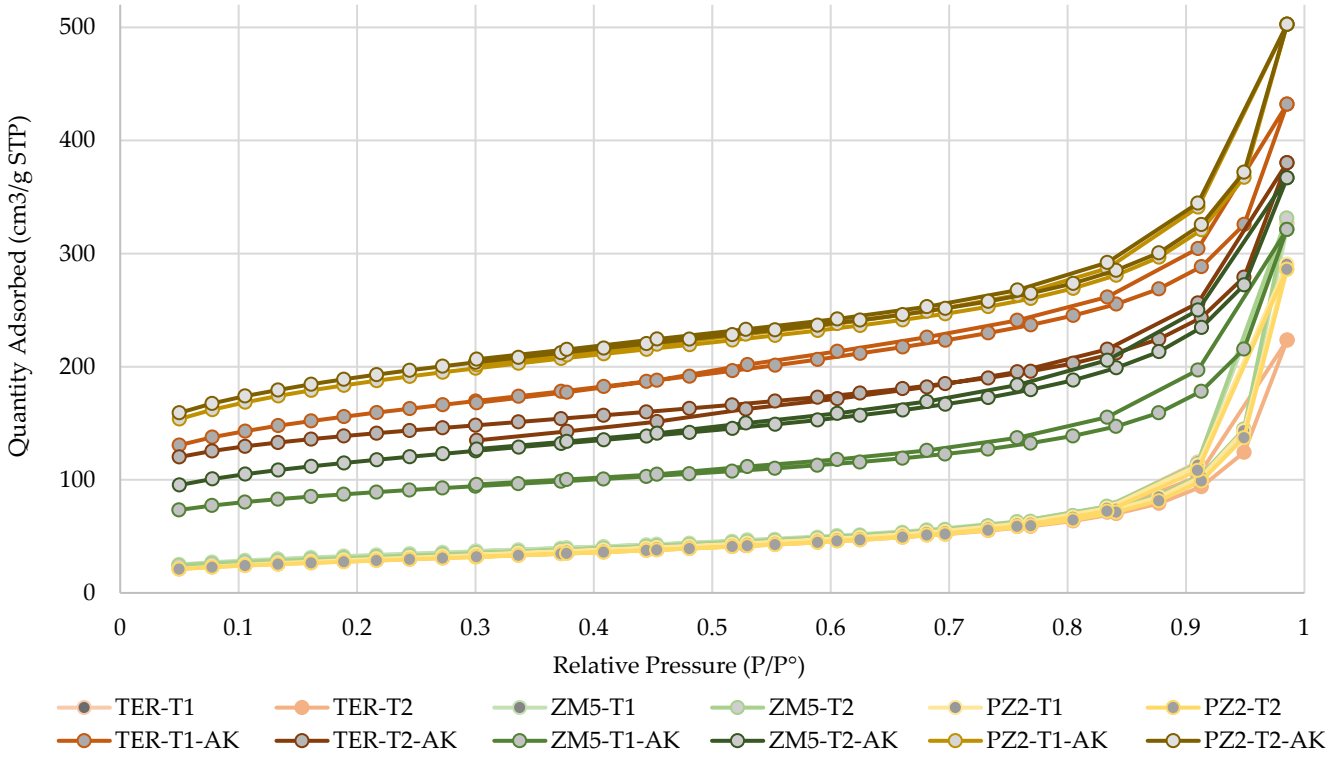


Figure 8. BET/Adsorption–desorption isotherms of N2 of carbons and activated carbon.

Likewise, the significant influence of chemical activation on the structural transformation of the material is evident, as shown by the reduction in A pore diameter and D pore diameter. This suggests the development of a finer and more optimized structure for adsorption. The presence of type IV isotherms with hysteresis loops in the PZ2-T1-AK and PZ2-T2-AK carbons confirms the coexistence of micropores and mesopores. This indicates that chemical activation not only reduces pore size but also improves pore distribution and accessibility, enhancing adsorption at both low and high relative pressures [40].

It is also necessary to highlight the role of the PZ2 catalyst as a key factor in the superior textural properties exhibited by PZ2-T1-AK and PZ2-T2-AK, in comparison with the other activated carbons. Although all carbons showed similar characteristics before activation, PZ2, unlike the commercial ZSM-5 zeolite, exhibited a higher content of amorphous phases, greater pozzolanic activity, and thermodynamic metastability. These features rendered it more reactive during activation, facilitating the formation of carbon with a higher propensity for micropore and mesopore development, ultimately resulting in higher BET surface areas, pore volumes, and specific surface areas. In contrast, ZSM-5, characterized by a more compact, highly crystalline structure, limited the generation of accessible sites for activation. Thus, although PZ2 has lower crystallinity, its metastable nature contributed to the production of activated carbons with larger BET surface areas [41].

In addition, activated carbons from other studies were considered for comparison. Notably, the physically activated carbon AC-CO_2 achieved an S_{BET} of 720 m^2/g and an SPSA of 514 m^2/g, significantly outperforming most activated carbons in this study. However, carbons such as AC-K (S_{BET}: 242 m^2/g; SPSA: 184 m^2/g) and AC-900 (S_{BET}: 328 m^2/g) presented intermediate surface areas that may still be valuable for specific applications. In contrast, materials like WTC 4M (S_{BET}: 63.07 m^2/g) and C-AC (S_{BET}: 86 m^2/g) exhibited considerably lower values, indicating more limited adsorption capacities. Among the chemically activated carbons, only AC-CO_2 showed slightly higher S_{BET} and ESA values than PZ2-T1-AK and PZ2-T2-AK, which, in turn, outperformed the rest.

The analysis of burn-off values further illustrates how porosity development is influenced by precursor type, activation temperature, reaction time, and the activating agent. Burn-off, which represents the fraction of carbonaceous material removed during activation, is directly related to the evolution of the porous structure. For instance, in carbons activated with KOH at 700 °C for 120 min, burn-off ranged from 43.68% (PZ2-T2-AK) to 64.45% (ZM5-T2-AK), highlighting the impact of both precursor characteristics and activation conditions [37]. Notably, all activated carbons achieved burn-off values above 40%, which is favorable for mesopore development [41]. Higher burn-off values were also observed at elevated temperatures, such as 54% for AC-K at 850 °C, while lower temperatures, such as 500 °C for C-AC, led to more limited pore formation [53]. Prolonged reaction times, like the 1680 min used for CO_2 activation (AC-CO_2), resulted in a moderate burn-off (50%), comparable to that obtained through chemical activation in shorter periods. Moreover, the choice of activating agent plays a crucial role: KOH yields moderate burn-off due to its strong ability to disrupt carbonaceous matrices and form micropores, while H_3PO_4 and CO_2 lead to more controlled carbon loss. These findings emphasize the importance of carefully optimizing activation parameters to enhance porosity while preserving material integrity.

3.3.2. Morphological Characterization of Activated Carbons Obtained by SEM

Figure 9 below presents the SEM images of WTC and its respective activated carbons.

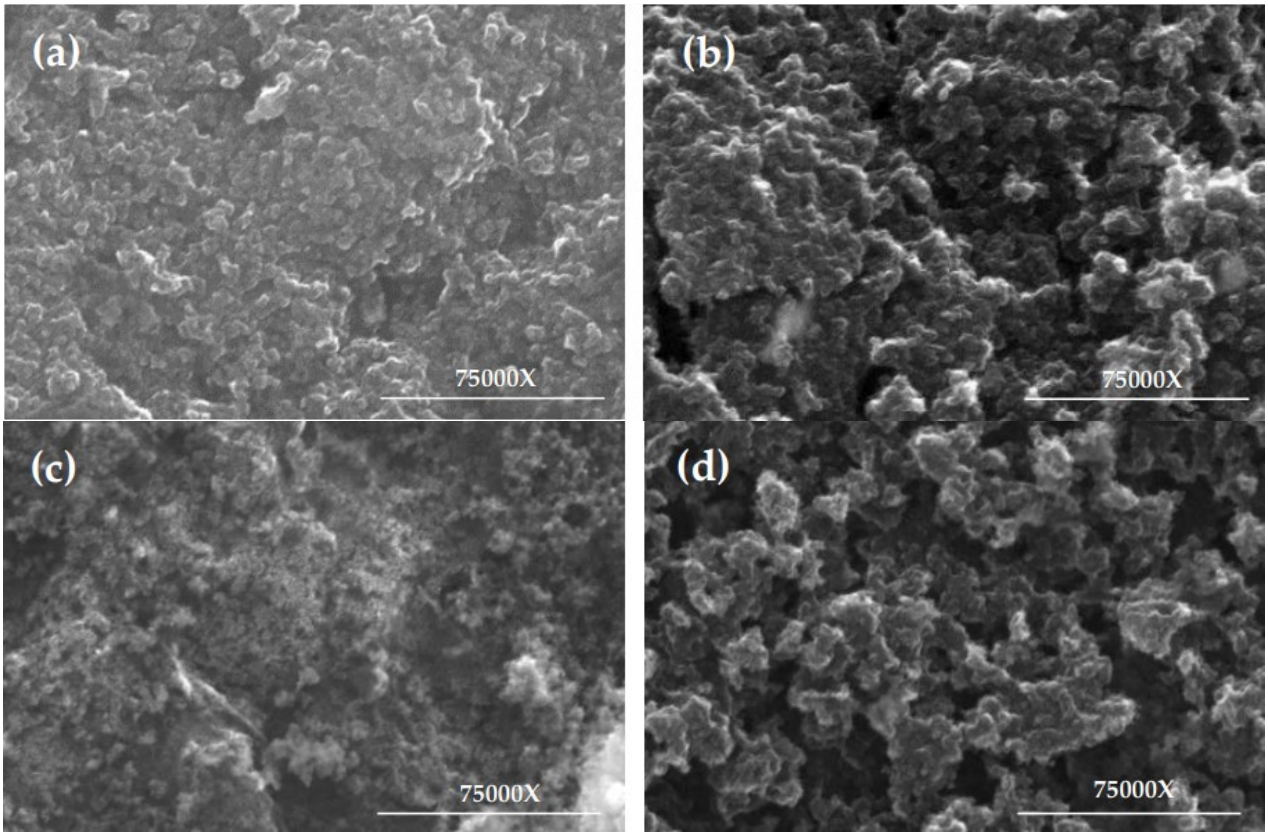


Figure 9. *Cont.*

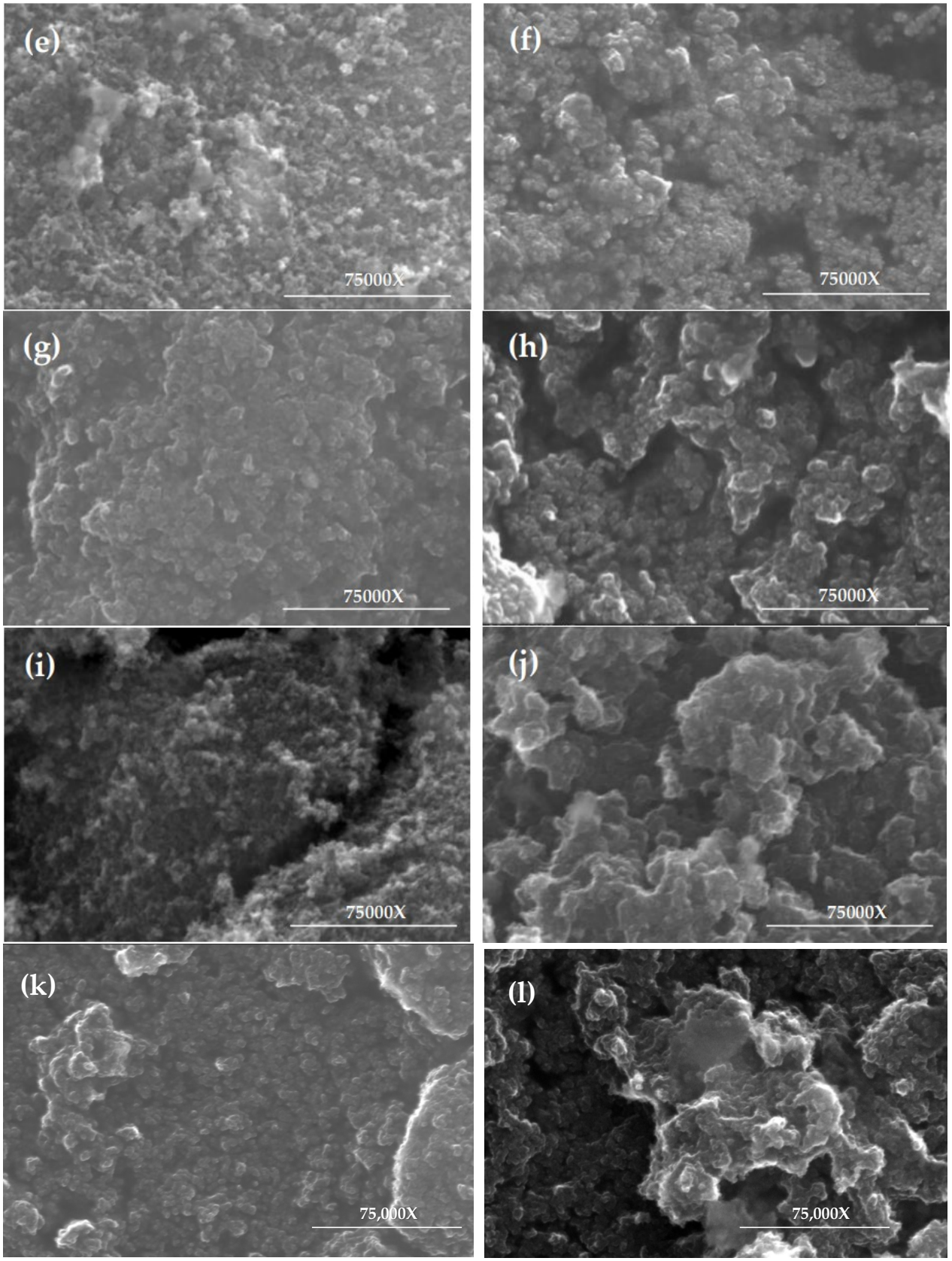


Figure 9. SEM (magnification 75,000×) of WTC and activated carbons. (**a**) TER-T1; (**b**) TER-T1-AK; (**c**) TER-T2; (**d**) TER-T2-AK; (**e**) ZM5-T1; (**f**) ZM5-T1-AK; (**g**) ZM5-T2; (**h**) ZM5-T2-AK; (**i**) PZ2-T1; (**j**) PZ2-T1-AK; (**k**) PZ2-T2; (**l**) PZ2-T2-AK.

SEM images of the activated carbons taken at 75,000x magnification clearly show an increased number of pores and interparticle spaces compared to their non-activated counterparts. Specifically, activated carbons such as TER-T1-AK and TER-T2-AK presented more prominent interparticle voids, while the non-activated samples (TER-T1 and TER-T2) appeared denser and more compact—a trend consistent across all non-activated materials. ZM5-T2-AK exhibited larger interparticle spaces than ZM5-T1-AK, although both showed enhanced porosity post-activation, with the latter displaying smaller and more tightly packed pores. Similarly, PZ2-T1-AK and PZ2-T2-AK exhibited pronounced interparticle spaces, suggesting a more open and porous structure resulting from the activation process.

These morphological changes are consistent with BET analysis, which confirms a significant increase in surface area and pore volume after activation. For example, TER-T1 increased from 105.65 m^2/g to 519.40 m^2/g in SBET, and its pore volume rose from 0.0004 cm^3/g to 0.1024 cm^3/g. TER-T2 also showed a marked increase in SBET from 99.24 m^2/g to 451.51 m^2/g, and in pore volume from 0.0041 cm^3/g to 0.1166 cm^3/g. ZM5-T1-AK and ZM5-T2-AK exhibited SBET values of 289.03 m^2/g and 385.30 m^2/g, respectively—substantially higher than their non-activated counterparts (114.50 m^2/g and 108.99 m^2/g). PZ2-T1-AK and PZ2-T2-AK showed the highest textural values, with SBET values of 608.65 m^2/g and 624.37 m^2/g, and pore volumes of 0.1248 cm^3/g and 0.1337 cm^3/g, respectively, in line with the extensive porosity observed in SEM.

Furthermore, differences in porosity and surface morphology can be linked to the initial structure of the zeolites used as catalysts. The SEM analysis of ZSM-5 revealed a compact hexagonal morphology with uniformly sized crystalline aggregates, implying a dense particle arrangement in the carbons derived from this material. This compactness likely contributed to the lower S_{BET} and M_{vol} values observed in the ZSM-5-based activated carbons. Conversely, PZ2 exhibited an octahedral morphology with clustered, rhombohedral structures and larger particle sizes, facilitating the development of a more open carbon structure after activation. The higher amorphous content of PZ2, as corroborated by XRD, likely played a role in its higher reactivity and more effective pore development during activation [47].

Overall, BET and SEM results consistently demonstrate that chemical activation enhances the porous structure of carbon materials. Additionally, the morphology and crystallinity of the zeolitic precursors significantly influence the activation outcome, affecting the accessibility and distribution of pores. These findings reinforce the importance of catalyst selection and activation conditions in tailoring the textural properties of activated carbons for adsorption applications.

4. Conclusions

The performance of WTC in pyrolysis remains stable (35.57–38.97%) without significant variations due to temperature or catalyst presence, indicating that increasing the temperature or including catalysts is not necessary to maximize carbon production, thereby reducing costs and energy consumption. Moreover, pyrolytic oil and gas yields exhibit an inverse relationship under the applied temperature conditions, with catalysts promoting cracking, though without drastic variations. Additionally, the structural stability of catalysts influences product distribution: more ordered structures facilitate cracking, while less ordered structures lead to variations in byproducts. These findings support the optimization of operating conditions based on the desired product.

According to the characterization of WTC and the activated carbons, in terms of surface area and volume, the best results were obtained for PZ2-T1-AK and PZ2-T2-AK, with BET surface areas of 608.65 m^2/g and 624.37 m^2/g, respectively. Furthermore, PZ2-T2-AK achieved a micropore volume of 0.1337 cm^3/g and a micropore area of

257.53 m^2/g. The CEC values for these carbons were remarkably high, ranging from 19.2 $cmol_c/kg$ (PZ2-T2-AK) to 21.0 $cmol_c/kg$ (PZ2-T1-AK), along with burn-off levels that indicate high material durability. When compared with activated carbons from other studies, those derived from PZ2 as a precursor exhibited superior physical properties. These properties are closely related to adsorption processes, particularly SPSA and SBET, which are critical parameters for evaluating the quality and performance of activated carbons. It is also important to highlight that chemical activation using KOH at the designated temperature contributed to achieving materials with desirable properties, suggesting that these activated carbons not only meet the requirements for adsorption applications but also present new opportunities for the development of highly efficient materials. Additionally, morphological analysis via SEM revealed that PZ2-T1-AK and PZ2-T2-AK possess a well-distributed and accessible structure, optimizing the mesoporous network due to the influence of the PZ2 zeolite, which is key for adsorption applications.

This study underscores the potential of waste tires for the production of activated carbons, promoting sustainable waste management and the development of functional materials for environmental remediation. Furthermore, it opens the door to exploring various catalysts and activation techniques to further enhance these carbons and expand the reuse of industrial waste in advanced adsorption materials, contributing to sustainability and the circular economy. For future research, it is recommended to explore different catalysts and activation strategies to develop even more efficient activated carbons, broadening their applicability in adsorption processes and reinforcing the valorization of industrial waste through the production of advanced materials.

Supplementary Materials: The following supporting information can be downloaded at: https://www.mdpi.com/article/10.3390/su17114822/s1, Table S1: Weights resulting from pyrolysis to obtain WTC; Table S2: Summary of the performance of by-products from pyrolysis of waste tires in the laboratory; Table S3: Activation process data for calculating burn-off.

Author Contributions: Conceptualization, investigation, and methodology, C.A.-C., R.C., K.M., and J.A.; writing—original draft preparation, C.A.-C.; writing—review and editing, C.A.-C., J.A., and R.C.; project administration and supervision, J.A. and R.C. All authors have read and agreed to the published version of the manuscript.

Funding: This research was financed by the Universidad Nacional de San Agustín de Arequipa-Perú with the project: "Functionalization of pyrolytic carbonaceous wastes obtained from polymeric wastes for adsorbent purposes" (contract number: IBA-001-2023-UNSA).

Data Availability Statement: The original contributions presented in the study are included in the article/Supplementary Materials, and further inquiries can be directed to the corresponding author.

Acknowledgments: The authors thank the Universidad Nacional de San Agustín de Arequipa-Perú through Contract No. IBA-001-2023-UNSA for its funding of this research.

Conflicts of Interest: The authors declare no conflicts of interest. The funders had no role in the design of the study, in the collection, analyses, or interpretation of data, in the writing of the manuscript, or in the decision to publish the results.

References

1. Al-Subari, L.; Ekinci, A. Strength and durability assessment of shredded tire rubber stabilized artificially cemented alluvial clay. *Constr. Build. Mater.* **2022**, *345*, 128312. [CrossRef]
2. Song, W.; Zhou, J.; Li, Y.; Li, S.; Yang, J. Utilization of waste tire powder for gaseous fuel generation via CO_2 gasification using waste heat in converter vaporization cooling flue. *Renew Energy* **2021**, *173*, 283–296. [CrossRef]
3. Chen, G.; Sun, B.; Li, J.; Lin, F.; Xiang, L.; Yan, B. Products distribution and pollutants releasing characteristics during pyrolysis of waste tires under different thermal process. *J. Hazard. Mater.* **2022**, *424*, 127351. [CrossRef]

4. Loloie, Z.; Mozaffarian, M.; Soleimani, M.; Asassian, N. Carbonization and CO_2 activation of scrap tires: Optimization of specific surface area by the Taguchi method. *Korean J. Chem. Eng.* **2017**, *34*, 366–375. [CrossRef]
5. Abdulai, A.; Owusu-Asenso, C.; Haizel, C.; Egyin, S.; Sraku, I.; Halou, D.; Doe, R.; Mohammed, A.; Akuamoah, Y.; Obeng, A.; et al. The role of car tyres in the ecology of Aedes aegypti mosquitoes in Ghana. *Curr. Res. Parasitol. Vector Borne Dis.* **2024**, *5*, 100176. [CrossRef]
6. Labaki, M.; Jeguirim, M. Thermochemical conversion of waste tyres—A review. *Environ. Sci. Pollut. Res.* **2017**, *24*, 9962–9992. [CrossRef]
7. Wang, M.; Zhang, L.; Li, A.; Irfan, M.; Du, Y.; Di, W. Comparative pyrolysis behaviors of tire tread and side wall from waste tire and characterization of the resulting chars. *J. Environ. Manag.* **2019**, *232*, 364–371. [CrossRef]
8. Pyshyev, S.; Lypko, Y.; Demchuk, Y.; Kukhar, O.; Korchak, B.; Pochapska, I.; Zhytnetskyi, I. Characcteristics and applications of waste tire pyrolysis products: A review. *Chem. Chem. Technol.* **2024**, *18*, 244–257. [CrossRef]
9. Dai, M.; Xu, H.; Yu, Z.; Fang, S.; Chen, L.; Gu, W.; Ma, X. Microwave-assisted fast co-pyrolysis behaviors and products between microalgae and polyvinyl chloride. *Appl. Therm. Eng.* **2018**, *136*, 9–15. [CrossRef]
10. Zhang, Y.; Li, S.; Zhang, Q.; Zhao, Y.; Liu, M.; Zhang, D.; Cai, X.; Wang, N.; Wang, W. Structural characterization and transformation of nitrogen compounds in waste tire pyrolysis oils. *J. Chromatogr. A* **2023**, *1702*, 464093. [CrossRef]
11. Hu, X.; Gholizadeh, M. Biomass pyrolysis: A review of the process development and challenges from initial researches up to the commercialisation stage. *J. Energy Chem.* **2019**, *39*, 109–143. [CrossRef]
12. Dick, D.T.; Agboola, O.; Ayeni, A.O. Pyrolysis of waste tyre for high-quality fuel products: A review. *AIMS Energy* **2020**, *8*, 869–895. [CrossRef]
13. Kusumo, P.; Romli, A.; Aulia, M.I.; Yanuar, E.M. Fuel Oil from Municipal Plastic Waste through Pyrolysis with and without Natural Zeolite as Catalysts. *ICENIS* **2018**, *2018*, 73.
14. Jana, S.K.; Pattanayak, S.; Bhausaheb, M.S.; Ruidas, B.C.; Pal, D.B. Pyrolysis of waste plastic to fuel conversion for utilization in internal combustion engine. *Chem. Chem. Technol.* **2023**, *17*, 438–449. [CrossRef]
15. Arabiourrutia, M.; López, G.; Aguado, R.; Olazar, M. Efecto del uso de catalizadores ácidos sobre la distribución de productos en la pirólisis de neumáticos. *Inf. Tecnol.* **2010**, *21*, 33–41. [CrossRef]
16. Lewandowski, W.M.; Januszewicz, K.; Kosakowski, W. Efficiency and proportions of waste tyre pyrolysis products depending on the reactor type—A review. *J. Anal. Appl. Pyrolysis* **2019**, *140*, 25–53. [CrossRef]
17. Sathiskumar, C.; Karthikeyan, S. Recycling of waste tires and its energy storage application of by-products—A review. *Sustain. Mater. Technol.* **2019**, *22*, e00125. [CrossRef]
18. Gao, N.; Wang, F.; Quan, C.; Santamaria, L.; Lopez, G.; Williams, P.T. Tire pyrolysis char: Processes, properties, upgrading and applications. *Prog. Energy Combust. Sci.* **2022**, *93*, 101022. [CrossRef]
19. Suhartono; Harsanti, M.; Septiyanti, W.; Suharto; Achmad, F. Zeolite catalytic pyrolysis of waste tire into fuel in gasoline hydrocarbon range. *IOP Conf. Ser. Earth Environ. Sci.* **2022**, *969*, 012030. [CrossRef]
20. Razzaq, G.H.A.; Majeed, N.S. Pyrolysis of scrap tire by utilizing zeolite as catalyst. *Mater. Today Proc.* **2021**, *45*, 4606–4611. [CrossRef]
21. Olazar, M.; Aguado, R.; Arabiourrutia, M.; Lopez, G.; Barona, A.; Bilbao, J. Catalyst effect on the composition of tire pyrolysis products. *Energy Fuels* **2008**, *22*, 2909–2916. [CrossRef]
22. Krasnovskikh, M.; Mokrushin, I.; Novoselov, K.; Kulikova, Y.; Toderas, M.; Bassyouni, M.; Babich, O. Recovered carbon black from tires as carbon carrier in metal oxide catalytic systems. *S. Afr. J. Chem. Eng.* **2024**, *49*, 64–72. [CrossRef]
23. Tang, L.; Huang, H. Thermal plasma pyrolysis of used tires for carbon black recovery. *J. Mater. Sci.* **2005**, *40*, 3817–3819. [CrossRef]
24. Kong, D.; Wang, S.; Shan, R.; Gu, J.; Yuan, H.; Chen, Y. Characteristics and chemical treatment of carbon black from waste tires pyrolysis. *J. Anal. Appl. Pyrolysis* **2024**, *178*, 106419. [CrossRef]
25. Dziejarski, B.; Hernandez-Barreto, D.; Moreno-Pirajan, J.C.; Giraldo, L.; Serafin, J.; Knutsson, P.; Andersson, K.; Krzyżyńska, R. Upgrading recovered carbon black (rCB) from industrial-scale end-of-life tires (ELTs) pyrolysis to activated carbons: Material characterization and CO_2 capture abilities. *Environ. Res.* **2024**, *247*, 118169. [CrossRef]
26. Selbes, M.; Yilmaz, O.; Khan, A.; Karanfil, T. Leaching of DOC, DN, and inorganic constituents from scrap tires. *Chemosphere* **2015**, *139*, 617–623. [CrossRef]
27. Chan, O.S.; Cheung, W.H.; McKay, G. Preparation and characterisation of demineralised tyre derived activated carbon. *Carbon N. Y.* **2011**, *49*, 4674–4687. [CrossRef]
28. Choi, G.G.; Jung, S.H.; Oh, S.J.; Kim, J.S. Total utilization of waste tire rubber through pyrolysis to obtain oils and CO_2 activation of pyrolysis char. *Fuel Process. Technol.* **2014**, *123*, 57–64. [CrossRef]
29. Miguel, G.S.; Fowler, G.D.; Sollars, C.J. The leaching of inorganic species from activated carbons produced from waste tyre rubbe. *Water. Res.* **2002**, *36*, 1939–1946. [CrossRef]

30. Ariyadejwanich, P.; Tanthapanichakoon, W.; Nakagawa, K.; Mukai, S.R.; Tamon, H. Preparation and characterization of mesoporous activated carbon from waste tires. *Carbon N. Y.* **2003**, *41*, 157–164. [CrossRef]
31. Alexandre-Franco, M.; Fernández-González, C.; Alfaro-Domínguez, M.; Gómez-Serrano, V. Adsorption of cadmium on carbonaceous adsorbents developed from used tire rubber. *J. Environ. Manag.* **2011**, *92*, 2193–2200. [CrossRef]
32. *ASTM E11-22*; Standard Specification for Woven Wire Test Sieve Cloth and Test Sieves. ASTM: West Conshohocken, PA, USA, 2022.
33. Wu, T.-L.; Chen, Y.-H.; Hsu, W.-D. Phase Transition Pathway of Hydrothermal Zeolite Synthesis. *Phys. Chem. Min.* **2021**, *48*, 1. [CrossRef]
34. Mamani, L.; Churata, R.; Valencia, A.; Fuentes, S.; Almirón, J. Comparison of the Synthesis Method of Zeolite Catalysts Based on Pozzolan, Pumice, and Ignimbrite Applied to the Sustainable Pyrolysis of Polymers. *Sustainability* **2025**, *17*, 2986. [CrossRef]
35. Jonzon, J. Characterization and modeling of amorphous and crystalline ratios in polyacrylates. Master Thesis, Engineering Chemistry, Mid Sweden University, Sundsvall, Sweden, 2020.
36. Sirinwaranon, P.; Sricharoenchaikul, V.; Vichaphund, S.; Soongprasit, K.; Rodchom, M.; Wimuktiwa, P.; Atong, D. Synthesis and characterization of the porous activated carbon from end-of-life tire pyrolysis for CO_2 sequestration. *J. Appl. Pyrolysis* **2023**, *174*, 106139. [CrossRef]
37. López, F.A.; Centeno, T.A.; Rodríguez, O.; Alguacil, F.J. Preparation and characterization of activated carbon from the char produced in the thermolysis of granulated scrap tyres. *J. Air Waste Manag. Assoc.* **2013**, *63*, 534–544. [CrossRef]
38. Bascomb, C. Rapid Method for the Determination of the Cation Exchange Capacity of Calcareous and Non-Calcareous Soils. *J. Sci. Food Agric.* **1964**, *15*, 821–823. [CrossRef]
39. Ćirić, V.; Prekop, N.; Šeremešić, S.; Vojnov, B.; Pejić, B.; Radovanović, D.; Marinković, D. The implication of cation exchange capacity (CEC) assessment for soil quality management and improvement. *Agric. For.* **2023**, *69*, 113–133.
40. Donohue, M.; Aranovich, G. Classification of Gibbs adsorption isotherms, Advances in Colloid and Interface Science. *Adv. Colloid Interfacce Sci.* **1998**, *76*, 137–152. [CrossRef]
41. Mohamed, H. Natural pozzolana as standalone photocatalyst for water treatment. *Inorg. Chem. Commun.* **2024**, *160*, 111981. [CrossRef]
42. Sousa, L.; Silva, A.; Silva, B.; Teixeira, C.; Arcanjo, A.; Frety, R.; Pacheco, J. Fast synthesis of ZSM-22 zeolite by the seed-assisted method of crystallization with methanol. *Microporous Mesoporous Mater.* **2017**, *254*, 192–200. [CrossRef]
43. Murukutti, M.; Jena, H. Synthesis of nano-crystalline zeolite-A and zeolite-X from Indian coal fly ash, its characterization and performance evaluation for the removal of Cs^+ and Sr^{2+} from simulated nuclear waste. *J. Hazard. Mater.* **2022**, *423*, 127085. [CrossRef]
44. Kokloku, B.; Awudza, J.; Mensah, M.; Rockso, M.; Kemausuor, F. Characterization of Ghanaian clays as raw materials for the synthesis of ZSM-5 zeolite. *Sci. Afr.* **2025**, *27*, e02570. [CrossRef]
45. Ramadhani, A.; Abdullah, I.; Krisnandi, Y. Effect of Physicochemical Properties of Co and Mo Modified Natural Sourced Hierarchical ZSM-5 Zeolite Catalysts on Vanillin and Phenol Production from Diphenyl Ether. *Bull. Chem. React. Eng. Catal.* **2022**, *17*, 225–239. [CrossRef]
46. Almirón, J.; Vargas, M.; Tupayachy, D.; Duquesne, S.; Roudet, F.; Silva-Vela, A. Influence of the Process of Synthesis of Zeolites from Volcanic Ash in Its Synergistic Action as a Flame-Retardant for Polypropylene Composites. *Buildings* **2022**, *12*, 24. [CrossRef]
47. Churata, R.; Almirón, J.; Vargas, M.; Tupayachy, D.; Torres, J.; Ortiz-Valdivia, Y.; Velasco, F. Study of Geopolymer Composites Based on Volcanic Ash, Fly Ash, Pozzolan, Metakaolin and Mining Tailing. *Buildings* **2022**, *12*, 1118. [CrossRef]
48. Kuśmierek, K.; Świątkowski, A.; Kotkowski, T.; Cherbański, R.; Molga, E. Adsorption on activated carbons from end-of-life tyre pyrolysis for environmental applications. Part I. preparation of adsorbent and adsorption from gas phase. *J. Anal. Appl. Pyrolysis* **2021**, *157*, 105205. [CrossRef]
49. Arabiourrutia, M.; Lopez, G.; Artetxe, M.; Alvarez, J.; Bilbao, J.; Olazar, M. Waste tyre valorization by catalytic pyrolysis—A review. *Renew. Sustain. Energy Rev.* **2020**, *129*, 109932. [CrossRef]
50. Jerzak, W.; Sieradzka, M.; Wądrzyk, M.; Magdziarz, A. Comparative study of grass pyrolysis over regenerated catalysts: Tyre ash, zeolite, and nickel-supported ash and zeolite. *Renew. Energy* **2024**, *236*, 121440. [CrossRef]
51. Pallarés, J.; González-Cencerrado, A.; Arauzo, I. Production and characterization of activated carbon from barley straw by physical activation with carbon dioxide and steam. *Biomass Bioenergy* **2018**, *115*, 64–73. [CrossRef]
52. Dong, T.; Ling, C.; Fu, L.; Xue, Y.; Pan, Y.; Zhang, Y.; Zhu, C. N-doped porous bowl-like carbon with superhigh external surface area for ultrafast degradation of bisphenol A: Key role of site exposure degree. *J. Hazard. Mater.* **2023**, *445*, 130562. [CrossRef]

53. El-Maadawy, M.; Elzoghby, A.; Masoud, M.; El-Deeb, M.; Naggar, A.E.; Taha, M. Conversion of carbon black recovered from waste tires into activated carbon via chemical/microwave methods for efficient removal of heavy metal ions from wastewater. *R. Soc. Chem.* **2024**, *14*, 6324–6338. [CrossRef] [PubMed]
54. Pedada, S.; Golagani, S.; Kumar, M.; Kumari, A. Study and characterization of Sterculia foetida (Java olive) activated carbon black Filled composite materials. *Results Chem.* **2025**, *13*, 102003. [CrossRef]

Disclaimer/Publisher's Note: The statements, opinions and data contained in all publications are solely those of the individual author(s) and contributor(s) and not of MDPI and/or the editor(s). MDPI and/or the editor(s) disclaim responsibility for any injury to people or property resulting from any ideas, methods, instructions or products referred to in the content.